communications biology

A Nature Portfolio journal

Article

https://doi.org/10.1038/s42003-025-09146-w

Recognition of two hydrophobic pockets in the KIX domain of CBP by FOXO4 transactivation domain

Jeongbeen Heo [1], Kyoung-Seok Ryu [2,3] & Chin-Ju Park [1]

The transcription machinery is assembled via interactions of DNA-bound transcriptional activators and coactivators. When the eukaryotic RNA polymerase II complex is formed, cAMP-regulated transcription factor (CREB) binding protein (CBP) acts as a general coactivator bridging the transcriptional apparatus. Forkhead box protein O4 (FOXO4), a transcription factor, has been reported to bind to the KIX domain of CBP (CBP-KIX). Although the CR3 of FOXO4 (FOXO4-CR3) binds as expected to the MLL and c-Myb sites of CBP-KIX, its substantially higher affinity for CBP, compared to its homolog FOXO3a, cannot be explained by a single conserved ΦXXΦΦ binding motif. Here, we found that a second ΦXXΦΦ motif in FOXO4-CR3 provides an additional point of contact for CBP-KIX. Isothermal titration calorimetry and chemical shift perturbation analyses revealed a difference in binding affinity and confirmed that different binding patterns occur at the two hydrophobic pockets of CBP-KIX. Increased helicity of FOXO4-CR3 upon KIX MLL site binding was demonstrated by circular dichroism and Cα chemical shifts. Paramagnetic relaxation enhancement and docking simulations suggested FOXO4-CR3 orientation is not restrained in the KIX-CR3 complex. Our study provides information about the unique binding properties of FOXO4-CR3 and CBP-KIX, expanding our understanding of CBP recruitment via KIX-transactivation domain binding.

The transcriptional machinery is assembled by interactions of DNA-bound transcriptional activators and coactivators with the components of the basal transcription complex[1]. cAMP-regulated transcription factor (CREB) binding protein (CBP), highly homologous to p300, is a histone acetyltransferase. It acts as a general coactivator for activator-dependent transcription by the eukaryotic RNA polymerase II complex, which binds the promoter[2–4]. CBP has multiple interaction domains, of which the KIX domain is a globular domain containing three α-helices, two short 3_{10}-helices (G1 and G2), and a well-folded hydrophobic core; KIX is highly conserved among the CBP homologs in yeast and animals (Fig. 1A)[5]. CBP contributes to target gene expression by binding to the phosphorylated KID domain (pKID) of CREB, a cellular transcription factor, via its KIX domain[3]. The KIX domain provides two isolated hydrophobic surfaces that can bind transactivation domains and can be occupied simultaneously (Fig. 1B)[6]. The docking site of both pKID and c-Myb is a binding groove that is formed by the first and third α-helices of CBP (the c-Myb site). In contrast, the docking site of MLL and Tax exists on the opposite side of the KIX domain (the MLL site)[7]. The electrostatic potential surface of KIX shows that the MLL site is more positively charged (Fig. 1C). KIX binding proteins share a ΦXXΦΦ motif, where "Φ" is a hydrophobic residue and "X" is an arbitrary residue[8].

Forkhead box (FOX) proteins are a large family of transcription factors involved in central biological processes, including proliferation, differentiation, stress resistance, DNA repair, cell cycle progression, apoptosis, and cellular metabolism[9–14]. The 'O' subgroup (FOXO) of the FOX family in mammals has the conserved region 3 (CR3), also known as the transactivation domain, which is rich in negatively charged amino acids and recruits coactivators such as CBP and p53 (Fig. 1D)[15,16]. Among FOXO proteins, FOXO4 is a crucial transcription factor involved in cellular senescence[17]. Although all FOXO proteins are maintained and controlled through the tight regulation of several signaling networks[13], when FOXO4 is out of regulatory control, the viability of senescent cells can cause cells to undergo carcinogenesis[17].

The biophysical processes of FOXO regulation revealed in multiple cell types involve regulating FOXO-dependent transcription by CBP[18]. The interaction between FOXO proteins and CBP's KIX domain was confirmed in DAF-16, the forkhead transcription factor in *Caenorhabditis elegans*, which recruits CBP to promote transcription[19].

[1]Department of Chemistry, Gwangju Institute of Science and Technology, Gwangju, Republic of Korea. [2]Ochang Center, Korea Basic Science Institute, Cheongju, Republic of Korea. [3]KBSI School of Bioscience, University of Science and Technology, Daejeon, Republic of Korea. e-mail: cjpark@gist.ac.kr

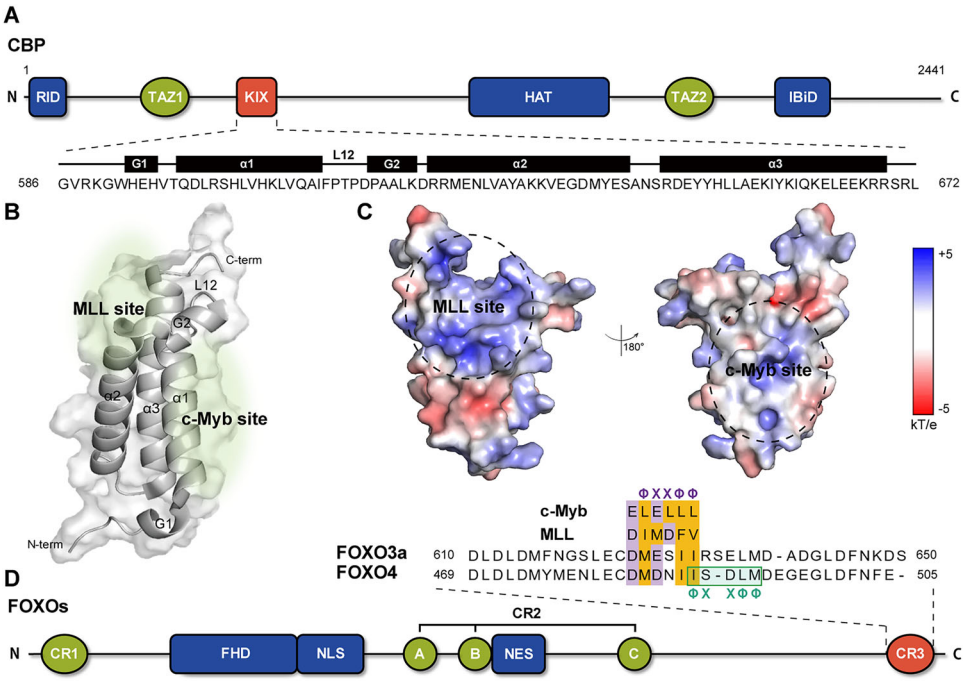

Fig. 1 | Schematic drawing of domains of CBP and FOXOs. A CBP consists of a nuclear receptor binding domain (RID), two transitional adapter zinc finger (TAZ) domains, a KIX domain, a histone acetyltransferase (HAT) domain, and an interferon binding domain (IBiD). **B** Structure of the KIX domain (PDB code: 2AGH) with c-Myb and MLL sites highlighted with light green on the surface and ribbon models. **C** Electrostatic potential surfaces of c-Myb and MLL sites on the KIX domain. The surfaces are colored according to the electrostatic potential from −5 (red) to +5 (blue) kT/e. The structural models were visualized with PyMOL. **D** FOXO proteins consist of a forkhead DNA binding domain (FHD), a nuclear localization signal (NLS), a nuclear export sequence (NES) and three C-terminal domains (CR1-CR3). Sequence alignments of the CR3 of FOXO3a and FOXO4, and the ΦXXΦΦ motif regions of c-Myb and MLL, are shown. The hydrophobic residues of the motif are colored yellow, and negatively charged residues are colored pink.

According to previous reports, human FOXO3a-CR3, which contains a ΦXXΦΦ motif, binds to CBP through its interaction with CBP-KIX[8,15] (Fig.1D). It has been shown that FOXO3a-CR3 promiscuously binds to both hydrophobic sites of CBP-KIX with similar binding affinities[15]. FOXO4, which is mainly expressed in skeletal and cardiac muscle, is highly similar to FOXO3a in its sequence and structural organization and also contains KIX-binding motifs in its CR3[14]. While the sequence homology between FOXO4-CR3 and FOXO3a-CR3 is significant, we found an additional ΦXXΦΦ motif in FOXO4-CR3 (Fig. 1D). It has been reported that p300 regulates FOXO4 activity and mRNA levels of its target genes in vivo[20], and an interaction between CBP and FOXO4 was reported using immunoprecipitation[21]. A previous study has shown that for FOXO4, a disulfide bond mediates interaction with CBP/p300 in the presence of reactive oxygen species[22]. While the essential cysteine involved in the intermolecular interaction is C481 in FOXO4-CR3, how the two proteins get close is not known. Because intrinsically disordered FOXO4-CR3 contains common KIX-binding motifs, we thoroughly investigated the biophysical properties of the interaction between CBP-KIX and FOXO4-CR3.

In this study, we confirmed the binding of FOXO4-CR3 and CBP-KIX through isothermal titration calorimetry (ITC) in vitro, which was much tighter than FOXO3a-CR3 – CBP-KIX binding. Also, our NMR chemical shift perturbation (CSP) analyses showed that FOXO4-CR3 can bind to both hydrophobic sites on CBP-KIX using both ΦXXΦΦ motifs, but with different structural and thermodynamic properties. Furthermore, we performed a series of experiments using KIX mutants strategically placed in the MLL and c-Myb binding sites to identify binding interfaces and observe changes in the binding affinity. Our study provides detailed information about FOXO4-CR3 and CBP-KIX interactions and gives insights into the interaction of FOXO4 and CBP during the formation of the eukaryotic RNA polymerase II complex.

Results

FOXO4-CR3 distinctly interacts with two hydrophobic surfaces of CBP-KIX

Even though the backbone atoms of CBP-KIX were already assigned (BMRB code: 26867 and 6095), they were not well matched to the NMR spectra obtained in our experimental conditions. We performed triple resonance experiments to complete the backbone assignments for KIX. Among 87 residues, 73 amide resonances were assigned (Supplementary Fig. S1). Unfortunately, a few residues in helix α3 (aa 656-659), part of the c-Myb site, could not be assigned due to severe overlap. Next, $^{1}H–^{15}N$ HSQC titration experiments identified the CR3 binding surface on KIX. Supplementary Fig. S2A shows the overlaid $^{1}H–^{15}N$ HSQC spectra of ^{15}N-labeled KIX during titration with CR3. Several residues showed significant CSPs upon CR3 addition. H605, V608, L664, and R671 showed $\Delta\delta_{avg}$ values of two standard deviations (S.D.) above the average, and T596, L620, G637, I660, S670, and L672 showed $\Delta\delta_{avg}$ values of one S.D. above the average (Fig. 2A). H605 and V608 are residues located in α1, L620 in G2, G637 in α2, and I660 and L664 in α3. In Fig. 2D, the three-dimensional structural mapping of KIX (PDB code: 2AGH) shows the positions of significantly perturbed residues. We found that most perturbed residues are in or near the two known MLL and c-Myb binding sites. Residues in the MLL site are I660, and L664; H605 is in the c-Myb site.

Next, we introduced mutations at the MLL site (I660A and L664A; MLL_{mut}) and c-Myb site (Y650A, A654Q, and Y658A; c-Myb_{mut}) of KIX to determine how the mutations influence FOXO4-CR3 binding. In previous studies, MLL and c-Myb site mutations were shown to effectively inhibit cognate ligands interacting at each binding site of KIX[15]. Mutations in the MLL site correspond to the highly perturbed residues in wild-type KIX (Fig. 2A). By comparing $^{1}H–^{15}N$ HSQC spectra of MLL_{mut} and c-Myb_{mut} with wild-type KIX, we confirmed that the mutation did not significantly change peak locations in the free protein except for the mutated residues

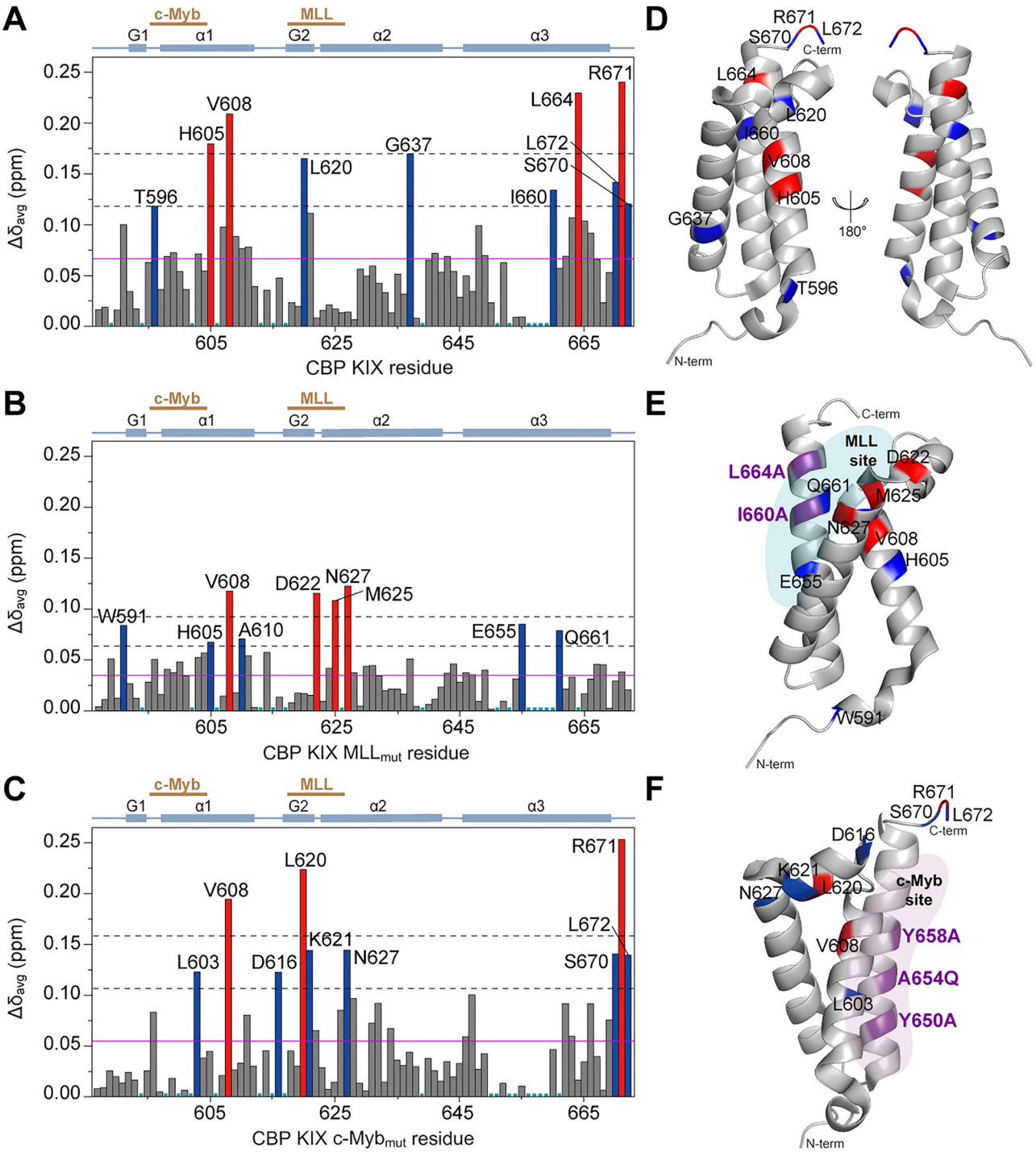

Fig. 2 | Chemical shift changes of CBP-KIX, KIX MLL_{mut}, and KIX c-Myb_{mut} upon titration with FOXO4-CR3. CSPs ($\Delta\delta_{avg}$) of ^{15}N-labeled **A** KIX, **B** MLL_{mut}, and **C** c-Myb_{mut} induced by 2.0 molar equivalents of CR3. The purple line indicates the average CSP. Thresholds for $\Delta\delta_{avg}$ values greater than average +1σ (lower) and 2σ (upper) are indicated by dashed lines. The residues with $\Delta\delta_{avg}$ values greater than average +2σ are colored in red, and $\Delta\delta_{avg}$ values greater than average +1σ are colored in blue. Mapping of residues affected by CR3 binding on the structure of **D** KIX, **E** MLL_{mut}, and **F** c-Myb_{mut} (PDB code: 2AGH). Residues perturbed by at least the average +2σ are shown in red, and those perturbed by at least the average +1σ are shown in blue. Mutated residues are shown in violet. The MLL site is shown in cyan and the c-Myb site is shown in magenta. The structural models were visualized with PyMOL.

(Supplementary Figs. S3, S4). In the case of c-Myb_{mut} spectrum, some line broadening and missing peaks were observed (Supplementary Fig. S4). ^{1}H–^{15}N cross-peak assignments of both mutants were completed by tracking from the ^{1}H–^{15}N HSQC spectrum of KIX (Supplementary Fig. S1).

The ^{1}H–^{15}N HSQC titration experiments identified the CR3-binding surface on KIX MLL_{mut}. Supplementary Fig. S2B shows the overlaid ^{1}H–^{15}N HSQC spectra of ^{15}N-labeled MLL_{mut} during titration with CR3. In the case of MLL_{mut}, the overall $\Delta\delta_{avg}$ decreased to 0.036, about half of the wild-type KIX. For identifying perturbed residues, the cutoff was defined using the overall the average +1σ of MLL_{mut} rather than the wild-type value. V608, D622, M625, and N627 showed $\Delta\delta_{avg}$ values of two S.D. above the average, and W591, H605, A610, E655 and Q661 showed $\Delta\delta_{avg}$ values of one S.D. above the average (Fig. 2B). Despite the mutations that were introduced in the MLL site, some residues in the MLL site (D622, M625, and N627)

showed a large perturbation of more than two S.D. above average. However, mutated residues that were greatly perturbed in α3 of wild-type KIX (I660 and L664) showed reduced chemical shift change. Together, these CSP patterns suggest that CR3 binding to MLL_{mut} may reflect not only direct binding but also structural or allosteric changes in KIX caused by blocking the MLL site. The significantly perturbed residues are mapped onto the structure of MLL_{mut} in Fig. 2E.

In the case of c-Myb_{mut}, the overall $\Delta\delta_{avg}$ was decreased less than in the MLL_{mut} case. V608, L620, and R671 showed $\Delta\delta_{avg}$ values of two S.D. above the average, and L603, D616, K621, N627, S670, and L672 showed $\Delta\delta_{avg}$ values of one S.D. above the average (Fig. 2C and Supplementary Fig. S2C). These residues are mapped onto the structure of c-Myb_{mut} in Fig. 2F. Notably, no or fewer perturbations were observed at the c-Myb site (T596 and H605), but residues constituting the MLL site (L620, K621, and N627) were rather perturbed compared to the apo form (Fig. 2A, C). Among them, N627 is located next to L628, a known key residue for MLL binding[23]. Our results show that c-Myb_{mut} effectively blocks the interaction that occurs at the c-Myb site.

Taken together, our data show that FOXO4-CR3 can interact with both the c-Myb and MLL sites on wild-type KIX. Impairment of the c-Myb site with mutations resulted in enhanced CSPs in the G2–α2 region of the MLL site. Also, significantly reduced CSP with MLL_{mut} suggests that the contribution of the MLL site to KIX-CR3 binding is important.

FOXO4-CR3 primarily binds to CBP-KIX through its second ΦXXΦΦ motifs

We found that FOXO4 has two consecutive ΦXXΦΦ motifs; the first motif is MDNII ($FOXO4_{483-487}$), and the second is ISDLM ($FOXO4_{487-491}$) (Fig. 1D). In the corresponding second motif region of FOXO3a-CR3, the hydrophobic residues "LM" are conserved, but FOXO3a-CR3 contains an extra X residue (Fig. 1D). While it is known that the first motif region is well conserved through various transactivation domains, the solution structure of the FOXO3a-CR3 – CBP-KIX complex showed that the conserved hydrophobic residues (L632 and M633) are also in the binding interface[15].

We performed NMR experiments to determine which regions of FOXO4-CR3 participate in KIX binding. $^{1}H–^{15}N$ HSQC titration experiments were performed with KIX titration into CR3, and Fig. 3A shows the overlaid spectra. Backbone atoms of FOXO4-CR3 were previously assigned (BMRB code: 50259)[24]. I487, S488, and M491 showed $\Delta\delta_{avg}$ values of two S.D. above the average, and D489 and L490 showed $\Delta\delta_{avg}$ values of one S.D. above the average (Fig. 3B). D492, located immediately after the second motif, underwent a significant perturbation more than the average to the extent that it was very close to the average +1σ. (1σ). These residues are clustered in the mid-late region of CR3. As most of these residues are aliphatic, it is considered that hydrophobic interactions are the dominant contribution to CR3 and KIX binding. However, the perturbation of acidic residues in their vicinity suggests that electrostatic attraction also contributes to the interaction between acidic CR3 (pI = 2.94) and basic KIX (pI = 9.61). Furthermore, a titration plot of residues in the ΦXXΦΦ motifs demonstrates the importance of I487 for binding to KIX (Supplementary Fig. S5).

We then performed an identical series of $^{1}H–^{15}N$ HSQC titration experiments with ^{15}N-labeled CR3 and unlabeled KIX mutants. The CSP analysis results for MLL_{mut} showed almost the same pattern as that of wild-type KIX. I487, S488, and M491 showed $\Delta\delta_{avg}$ values of two S.D. above the average, and D489, L490, and D492 showed $\Delta\delta_{avg}$ values of one S.D. above the average (Fig. 3C, D). On the other hand, the CSP analysis of c-Myb_{mut} differed from the wild-type KIX and MLL_{mut} data (Fig. 3E, F). I487 and D489 showed $\Delta\delta_{avg}$ values of two S.D. above the average, and D492 showed an $\Delta\delta_{avg}$ value of one S.D. above the average. The $^{1}H–^{15}N$ cross-peak corresponding to S488 disappeared during the titration. Residues that were barely affected in KIX and MLL_{mut} experiments were perturbed enough to undergo changes corresponding to almost the average +1σ in c-Myb_{mut} experiments (Fig. 3E, F). For this reason, the average value of perturbation increased to about twice that of MLL_{mut}, and the overall perturbations increased in all areas. This region includes several acidic residues and the first ΦXXΦΦ motif. In the second motif, hydrophobic residue perturbation was reduced, and acidic residue perturbation was maintained. Additionally, we investigated the interaction of CR3 at the MLL site after disrupting the motif by alanine substitution of M491 (M491A), the last residue of the second motif (Supplementary Fig. S6). Similar to wild-type CR3, I487 and S488 showed significant perturbations, whereas the perturbations in the first motif interaction were relatively reduced. The observation that a residue in the second motif affects CSPs of the first motif suggests potential allosteric communications between the two motifs.

Based on our results, we suggest that CR3 interacts with KIX through the second ΦXXΦΦ motif mainly when the c-Myb site is present (i.e., in the case of wild-type KIX and MLL_{mut}). However, when the c-Myb was mutated, we observed that the binding site in CR3 was not restricted to the second ΦXXΦΦ motif. The interaction affects a broader region, including several acidic residues and the first and second ΦXXΦΦ motifs.

Two hydrophobic sites of KIX are driven by different thermodynamics

We conducted ITC experiments to observe the differences in thermodynamic parameters of CR3 binding to the two binding sites of KIX (Supplementary Fig. S7, Table 1, and Supplementary Table S1). All ITC experiments were performed by titrating KIX or KIX mutants into CR3.

Firstly, we investigated the binding of KIX mutants to FOXO4-CR3. Table 1 shows that the K_ds of MLL_{mut} and c-Myb_{mut} were 2.76 ± 0.58 μM and 1.20 ± 0.50 μM, respectively. Interestingly, the released heat of binding with c-Myb_{mut} was significantly smaller than those of MLL_{mut} (Fig. 4). The enthalpies were −5.98 ± 0.75 kJ/mol for c-Myb_{mut} and −19.16 ± 2.51 kJ/mol for MLL_{mut}; the enthalpy of MLL_{mut} is about three times greater than that of c-Myb_{mut}. The entropies were 93.10 ± 4.21 J/mol·K for c-Myb_{mut} and 42.30 ± 9.20 J/mol·K for MLL_{mut}; the entropy of c-Myb_{mut} is about two times greater than that of MLL_{mut} (Fig. 4). These thermodynamic results suggest that when CR3 interacts with KIX, the binding is mainly driven entropically for the MLL site and enthalpically for the c-Myb site.

The measured thermodynamic parameters for wild-type KIX – CR3 binding were similar to those for MLL_{mut} – CR3 (Supplementary Table S1). Because of the distinct thermodynamic properties of the two binding sites, ITC could not clearly distinguish between the binding pockets of KIX (Fig. 4). Therefore, we applied the 1:1 binding model, as in the analyses of the KIX mutants, and obtained a K_d of 3.35 ± 0.14 μM, which falls within the range observed for the individual binding sites. However, we suggest that the values should be cautiously used because the isotherm of wild-type KIX could be a mixture of each isotherm for two binding sites, and it affects the slope of the isotherm.

Partial α helix is induced in CR3 when complexed with KIX MLL site

When an intrinsically disordered protein binds to its partner, a more folded conformation is often induced. Helicity was increased in the MLL and c-Myb sites, as well as in the CR2C or CR3 peptides of FOXO3a, upon binding of KIX[15,25]. To investigate the secondary structural change of FOXO4-CR3 upon binding, circular dichroism (CD) spectroscopic experiments were performed (Fig. 5). The domains of KIX and its mutants showed typical patterns of α-helix proteins with negative bands at 222 nm and 208 nm. They were expected to have more than 50% helical propensity (Fig. 5), in agreement with the known three-dimensional structure of KIX. The measured CD spectrum of CR3 predicted it to be more than 98% intrinsically disordered (Fig. 5), also consistent with its known transient structural properties as an intrinsically disordered protein[26]. By subtracting the molar ellipticity values of KIX or KIX mutants from KIX–CR3 complexes, we obtained 'calculated CR3' spectra. All calculated curves for CR3s had greater helicity than spectra for free CR3. Helicity gains of 7.9%, 2.9%, and 18.0% were estimated for CR3 upon binding to KIX, MLL_{mut}, and c-Myb_{mut} (Fig. 5). Even when CR3 bound to the c-Myb site, helix was rarely induced, but the binding pocket with the most helix formation was the MLL

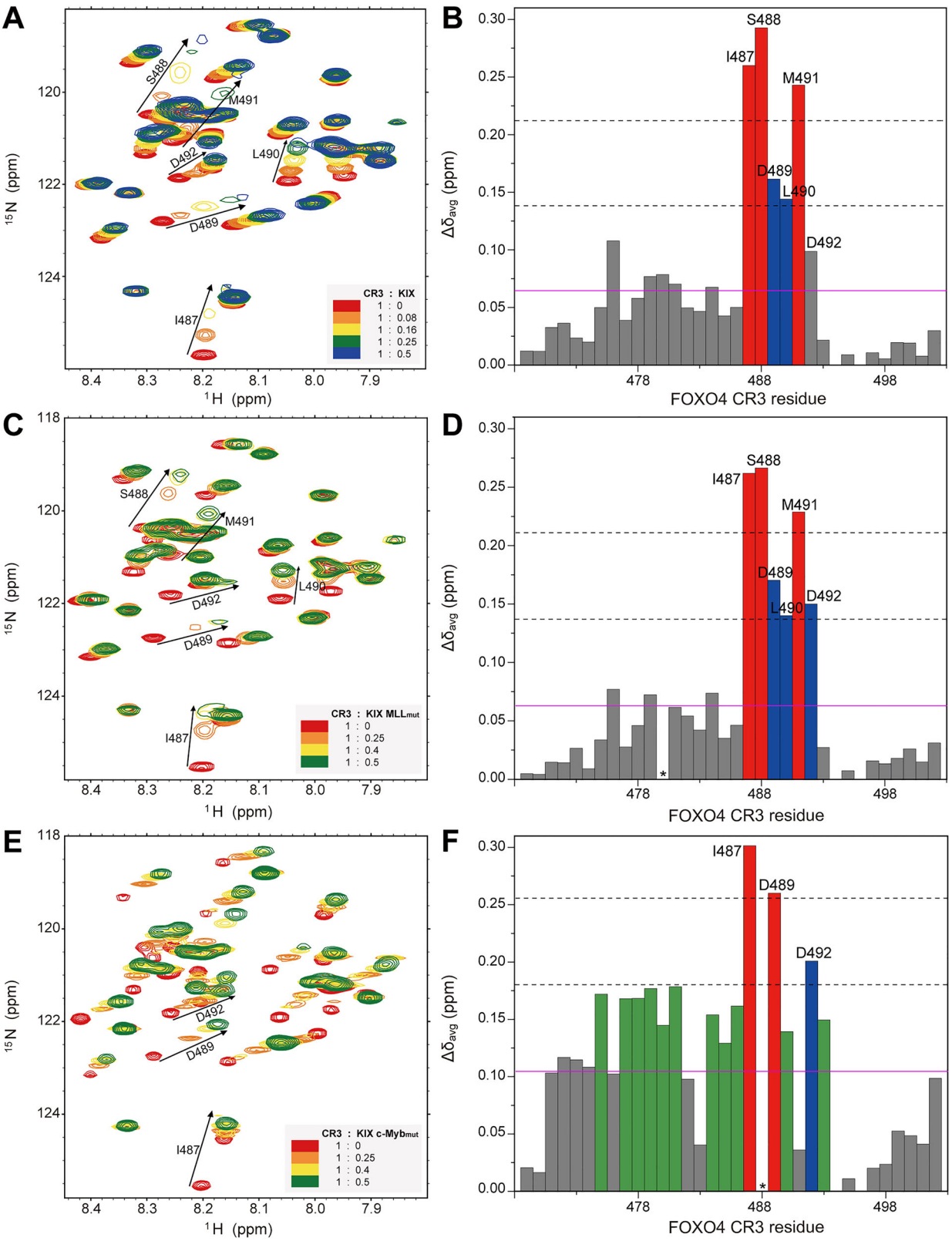

Fig. 3 | Chemical shift changes of FOXO4-CR3 in the presence of KIX and KIX mutants. Left: Overlaid ^{1}H–^{15}N HSQC spectra of ^{15}N-labeled CR3 at increasing molar ratios of **A** KIX, **C** KIX MLL_{mut}, and **E** KIX c-Myb_{mut}. Right: CSPs ($\Delta\delta_{avg}$) of ^{15}N-labeled CR3 induced by 0.5 molar equivalents of **B** KIX, **D** KIX MLL_{mut}, and **F** KIX c-Myb_{mut}. The purple line indicates the average CSP. The thresholds for average +1σ (lower) and 2σ (upper) are indicated by dashed lines. The residues with $\Delta\delta_{avg}$ values greater than average +2σ are colored in red, $\Delta\delta_{avg}$ values greater than average +1σ are colored in blue, and $\Delta\delta_{avg}$ values greater than average +0.4σ are colored in green. Asterisks indicate residues with disappeared peaks in the spectrum with KIX or KIX mutants.

Table 1 | Thermodynamic parameters of FOXO4-CR3 with KIX mutants

	K_d(μM)	Δ*G*(kJ/mol)	Δ*H*(kJ/mol)	-*T*Δ*S*(kJ/mol)	Δ*S*(J/mol·K)
KIX MLL_{mut}	2.76 ± 0.58	−31.78 ± 0.51	−19.16 ± 2.51	−12.61 ± 2.74	42.30 ± 9.20
KIX c-Myb_{mut}	1.20 ± 0.50	−33.74 ± 1.09	−5.98 ± 0.75	−27.75 ± 1.25	93.09 ± 4.21

Values are the means and standard deviations calculated from at least quadruplicate experiments.

site. Considering the length of CR3 (37 aa), we estimated that around two turns of α-helix were induced upon the MLL site binding. This suggests that α-helical structure is gained by CR3 under all conditions in complex with KIX, and the MLL site was more involved in its formation than the c-Myb site.

To determine where the α-helix was formed within FOXO4-CR3 upon CBP-KIX binding, we measured Cα chemical shifts in the presence of KIX c-Myb_{mut} at a 1:1 molar ratio (Fig. 6). Experiments were performed with KIX c-Myb_{mut}, which is the most favorable condition for the α-helix formation in CR3 (Fig. 5C). $\Delta\delta C_\alpha$ was calculated by subtracting free Cα chemical shift values from the measured Cα in the presence of KIX c-Myb_{mut}. $\Delta\delta C_\alpha$ of $CR3_{472\text{-}492}$ have continuous positive values. In particular, the region corresponding exactly to the first and second ΦXXΦΦ motifs ($FOXO4_{483\text{-}491}$) was perturbed more than the average. This means that when these nine residues bind to the MLL site, an α-helix of around 2.5 turns is induced with a high probability, consistent with the result observed by CD spectroscopy.

CR3 likely adopts unconstrained orientation at the KIX MLL site

Having established the helical formation of CR3 at the MLL site, we next investigated its binding orientation using paramagnetic relaxation enhancement (PRE) experiments. As KIX c-Myb_{mut} lacks cysteine residue, we introduced cysteine into the N-terminus (C585) or C-terminus (S670C) of KIX c-Myb_{mut}. These mutants, KIX c-Myb_{mut} C585 and KIX c-Myb_{mut} S670C, were labeled with S-(1-oxyl-2,2,5,5-tetramethyl-2,5-dihydro-1H-pyrrol-3-yl) methyl metheransulfonothioate (MTSL) (Supplementary Fig. S8). Under the experimental conditions, it was confirmed that MTSL has no detectable interaction with either CBP-KIX or FOXO4-CR3 (Supplementary Fig. S9). The paramagnetic broadening of peaks on ^1H–^{15}N HSQC spectra of FOXO4-CR3 was quantified as intensity ratio ($I_{paramagnetic}/I_{diamagnetic}$).

For KIX c-Myb_{mut} residues C585 (The N-terminal spin label), residues D471, M476, L490, L497, and F501 of CR3 exhibited reduced intensity ratios ($I_{paramagnetic}/I_{diamagnetic} < 0.50$) (Fig. 7A). In the case of KIX c-Myb_{mut} S670C (The C-terminal spin label), residues D471, L472, M476, E477, N478, L479, C481, D482, I486, I487, L490, L497, F499, N500, F501, and E502 of CR3 showed reduced intensity ratios ($I_{paramagnetic}/I_{diamagnetic} < 0.50$) (Fig. 7B). The ^1H–^{15}N cross-peak corresponding to S488 was not observed under KIX c-Myb_{mut} – CR3 mixture conditions, consistent with the ^1H–^{15}N HSQC titration experiments (Fig. 3E, F). Intensity reductions were primarily observed in the C-terminal region, ΦXXΦΦ motifs, and its preceding residues, including those mainly affected in the KIX c-Myb_{mut} C585 experiment (Fig. 7A).

Based on the observation that CR3 could form a partial α helical structure at the ΦXXΦΦ motif region, we mapped the location of affected residues on the helical wheels. The helical wheels show that the side chains of these residues from both N- and C- labeling, except for each terminal, are oriented in the same direction (Supplementary Fig. S10). In particular, KIX c-Myb_{mut} S670C affects residues I486, I487, and L490 of the ΦXXΦΦ motif, which are positioned on the same face of the helical wheel (Supplementary Fig. S10B). While the C-terminal spin-label of KIX affected more CR3 residues, particularly in and around the ΦXXΦΦ motif region, the central location of these motifs in the CR3 sequence makes it difficult to determine a definitive orientation of CR3 at the MLL site. Moreover, the residues influenced by MTSL at each terminus are not entirely distinct, and some regions may have overlapping effects from both labels, the data must be carefully interpreted (Supplementary Fig. S8).

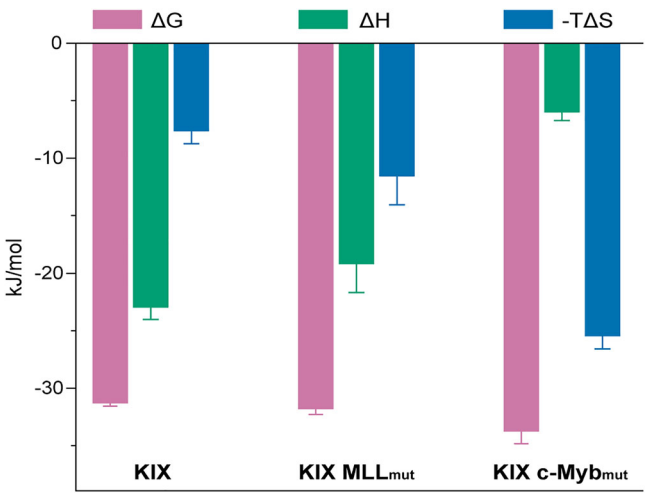

Fig. 4 | Thermodynamic analysis of FOXO4-CR3 complex formation with CBP-KIX and KIX mutants. The Gibbs free energy change (ΔG) is colored in pink, the enthalpy change (ΔH) is colored in green, and the entropy change (expressed as -TΔS) is colored in blue. Error bars represent the standard deviations of at least quadruplicate experiments.

To gain further insights into CR3-MLL site interaction, we performed complementary PRE experiments with MTSL-labeled C481 of the CR3 and ^{15}N-labeled KIX c-Myb_{mut}. Multiple KIX residues exhibited reduced intensity ratios ($I_{paramagnetic}/I_{diamagnetic} < 0.50$) or were broadend beyond detection (Fig. 7C). The significant interactions with C481 spin label were localized to the MLL site and G2-front of α2, with minimal effects at the N-terminus and its adjacent α2 rear region (Fig. 7D). These widespread PRE effects observed on KIX c-Myb_{mut}, combined with our findings showing dispersed effects on CR3, indicate that the binding orientation of CR3 is not fully constrained, which might be related to its micromolar K_d to KIX.

Structural modeling suggests consistent positioning of ΦXXΦΦ motifs between α2 and α3 of KIX

Given the challenges in obtaining crystals and severe peak overlap in NMR spectra of the KIX c-Myb_{mut} and CR3 complex using 8aa (KIX c-Myb_{mut}-linker-CR3 construct), we employed AlphaFold3 to model the interaction between CBP-KIX and FOXO4-CR3 (Fig. 8). Multiple simulations were conducted using random seeds, and the 13 complex models (pTM > 0.66, ipTM > 0.45) were selected. When one CR3 was docked to KIX, all models showed CR3 bound to the MLL site. Notably, all models exhibited CR3 with a higher helical content than experimentally confirmed. Our CD spectroscopy results and Cα CSP data also support a hypothesis of enhanced helicity at the MLL site (Figs. 5 and 6), even though there is a discrepancy in the length of the induced α-helix.

The CR3 models binding to the MLL site demonstrated two distinct orientations: three models showed the N-terminus of CR3 facing the C-terminus of KIX, while the remaining ten had the C-terminus of CR3 oriented towards the C-terminus of KIX (Fig. 8A). The three models with highest quality predictions (pTM > 0.74, ipTM > 0.59) are included in these ten models. Intriguingly, the spatial locations of ΦXXΦΦ motifs were consistent in 11 out of 13 models, with the ten models with their C-terminus pointing toward the C-terminus of KIX were exactly identical, down to the

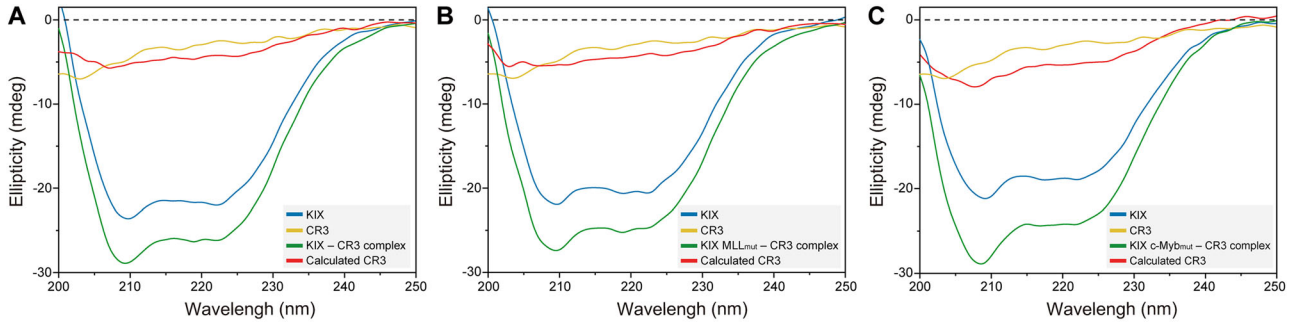

	Helicity (%)
KIX	55.6
CR3	7.9

	Helicity (%)
KIX MLL$_{mut}$	55.2
CR3	2.9

	Helicity (%)
KIX c-Myb$_{mut}$	51.0
CR3	18.0

Fig. 5 | CD spectra of each complex. CD spectra for **A** KIX, **B** KIX MLL$_{mut}$, and **C** KIX c-Myb$_{mut}$ (blue line), along with CR3 (yellow line), the respective KIX – CR3 complexes (green line), and the respective calculated CR3s (red line), were measured from 200 to 250 nm. Calculated CR3s represent the difference in ellipticity between the KIX domains and KIX – CR3 complexes at each wavelength. Percent helicities were calculated using BeStSel.

positions of their residues. This suggests that the region prone to helix formation upon binding to the MLL site is likely situated between α2 and α3 of KIX (Fig. 8B). The localized clustering of hydrophobic residues identified in the PRE experiment (Supplementary Fig. S10) forms tight hydrophobic interactions with I611 and F612 between α1 and G2, L628 and Y631 in α2, and L664 in α3 of KIX (Supplementary Fig. S11). In particular, L628 of KIX, a pivotal residue for MLL binding, is located within 5 Å of I486, I487, and L490 of CR3. The consistent positioning of I486, I487, and L490 in both the AlphaFold model and the PRE-based helical wheel supports the validity of the predicted binding interface (Supplementary Figs. S10B, S11). The reliability of these models can be further strengthened by previous findings that hydrophobic residues of KIX are energetically more important in the MLL site[23]. Although these predictions may have limited accuracy (ipTM = 0.45 < 0.6, which is below the general threshold of 0.6 for high confidence), they provide additional structural insights into the variable binding orientations of CR3.

Discussion

In this study, we investigated the binding of FOXO4-CR3 and CBP-KIX using NMR, ITC, CD, and modeling techniques. Consistent with prior research demonstrating that the intrinsically disordered regions of other transactivation domains bind to the two hydrophobic pockets in CBP-KIX[6,8,15], our NMR study showed that FOXO4-CR3 perturbs residues mainly clustered at the c-Myb and MLL sites of KIX (Fig. 2A). Even though c-Myb$_{mut}$ and MLL$_{mut}$ were not designed to block FOXO4-CR3 binding, we found that these mutations affect CR3 binding distinctively (Fig. 2B, C). In particular, the overall CSPs were markedly reduced in KIX MLL$_{mut}$ compared to wild-type. This reduction may partly result from the unassigned residues in the α3 helix, which limit the detection of perturbations at the c-Myb site, and may also reflect an allosteric influence of the disrupted MLL pocket on the overall CR3 binding mode.

Previous studies have shown that KIX has binding cooperativity. In silico experiments to reveal the dynamic behavior of CBP-KIX with MLL or CREB (pKID) suggest that when the MLL is bound, the conformational ensemble containing the c-Myb site is redistributed in response to the formation of this complex[27]. The binding of the first ligand to the MLL site induces opening of the hydrophobic core due to the dynamic change of the L12 loop, which subsequently increases the binding strength and stability of the complex at the other site[25,28]. An additional comparison of the apo and CR3-bound structures of KIX and KIX mutants predicted with AlphaFold2-multimer suggests that there may be similar differences in the rotation of L12-G2 (Supplementary Fig. S12). In addition, molecular dynamics simulations demonstrated that stronger allosteric communication is formed upon c-Myb•KIX•MLL ternary complex formation arising from MLL binding first[29]. Therefore, the binding of c-Myb and MLL is cooperative,

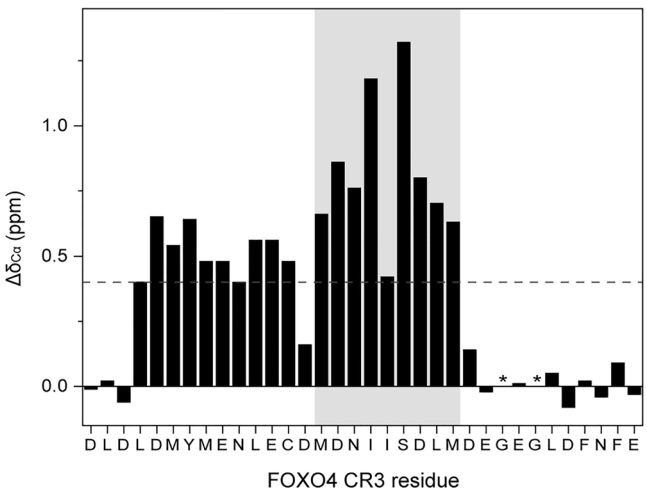

Fig. 6 | The chemical shift index of α carbon of FOXO4-CR3 upon binding to KIX c-Myb$_{mut}$. $\Delta\delta_{C\alpha}$ was calculated as the difference from the Cα of FOXO4-CR3 (BMRB code: 50259). The first and second ΦXXΦΦ motifs are indicated using the gray background. Dashed line indicates the average. Asterisks indicate that residues are not assigned.

indicating allosteric regulation between the two binding grooves. This explains why unintended residues were affected in the CSP analyses of the mutants (Fig. 2B, C). The decrease in the overall $\Delta\delta_{avg}$ of MLL$_{mut}$ indicates that mutation at the MLL site may weaken not only direct binding but also the accompanying structural rearrangement (Fig. 2B). c-Myb$_{mut}$ showed line broadening and missing peaks in the apo state (Supplementary Fig. S4), but displayed more extensive perturbations upon CR3 titration (Supplementary Fig. S2C). These suggest that CR3 binding to the MLL site can partly stabilize the c-Myb$_{mut}$ complex, reinforcing the cooperative and allosteric communication between the two binding sites.

Our CD data (Fig. 5) and docking predictions (Fig. 8) also indicate that FOXO4-CR3 exhibits a preferential binding for the MLL site. Simulation models have been proposed that other binding partners of KIX also bind to the MLL site first[25,30]. We found the positions of the central residues on the ΦXXΦΦ motifs that interact closely with L628., which plays an important role in the conformational transition of the MLL region[23]. Here, I486, I487, and L490 of motifs further stabilize the complex by interacting not only with L628 of α2 but also with hydrophobic residues of other helices (Supplementary Fig. S11). The hydrophobic interactions observed in our modeling are consistent with those found in the crystal structure of KIX-FOXO3a CR2C-CR3 complex (PDB code: 2LQH)[15]. Unlike FOXO4-CR3,

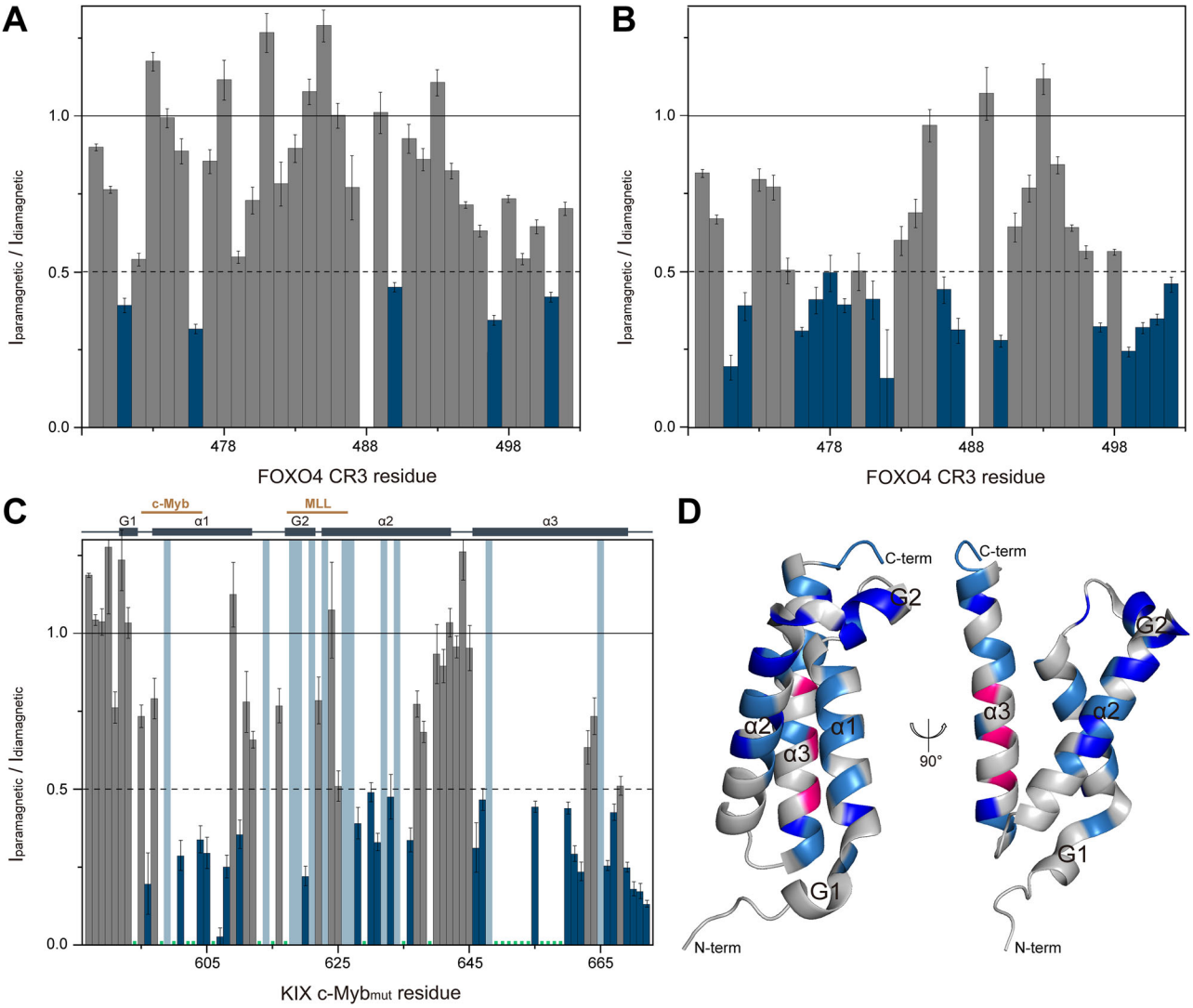

Fig. 7 | Results of PRE experiments between CBP-KIX c-Myb$_{mut}$ and FOXO4-CR3. Plots of the reduction intensity ratio ($I_{paramagnetic}$ / $I_{diamagnetic}$) of FOXO4-CR3 signals against the residue number are shown for FOXO4-CR3 in complex with CBP-KIX c-Myb$_{mut}$ modified with MTSL at **A** C585 or **B** S670C. The residues with reduction intensity ratio less than 0.5 are colored in blue. **C** Plots of the reduction intensity ratio of CBP-KIX c-Myb$_{mut}$ signals against the residue number are shown for CBP-KIX c-Myb$_{mut}$ in complex with FOXO4-CR3 modified with MTSL at C481. Residues with reduction intensity ratio less than 0.5 are colored in blue, and those broadened out under the influence of MTSL are indicated using the light blue. **D** Mapping of residues affected by MLSL labeled CR3 on the structure of KIX c-Myb$_{mut}$ (PDB code: 2AGH). Residues with reduction intensity ratio less than 0.5 are shown in light blue, and those broadened out under the influence of MTSL are indicated shown in blue. Mutated residues are shown in pink. Error bars represent the reciprocal of the signal-to-noise ratio for each residue. The structural models were visualized with PyMOL.

FOXO3a-CR3 shows non-selective binding to both c-Myb and MLL sites of KIX, with much lower binding affinities and no preferred orientation. Although CR3 is conserved within the FOXO family and likely adopts similar bound conformations, subtle sequence differences between family members may lead to distinct binding properties. Even with current modeling techniques, it is challenging to simulate protein complex formation when multiple binding sites are involved. Further studies are needed to determine whether the binding of FOXO4-CR3 to KIX results in dynamic behavior via an allosteric effect.

As an intrinsically disordered region, FOXO4-CR3 has multiple binding partners. This region is also known to participate in binding with its own FHD and p53 DNA binding domain (DBD)[24,31]. FOXO4 FHD, p53 DBD, and CBP-KIX commonly use the central region of CR3 as an interaction site, with FOXO4$_{487-491}$ (second ΦXXΦΦ motif) being the primary binding site. While the hydrophobic interactions are crucial in maintaining all of these complexes, the electrostatic interactions between the acidic residues of CR3 and the basic residues of FHD, p53 DBD, and CBP-KIX also play an important role. The flexible nature of CR3 as an intrinsically disordered region allows it to interact with the binding surfaces of various domains. In the process, the increase in the helical content of CR3 may promote more efficient and stable complex formation by the electrostatic interactions[25]. In particular, considering that the binding to KIX is predominantly via electrostatic interaction, the dominance of the interaction between the ΦXXΦΦ motif and the more positively charged MLL site becomes apparent (Fig. 1C).

Our study also reveals FOXO4-CR3 adopts different binding modes on KIX, exemplifying its promiscuous nature. This molecular promiscuity has significant implications for understanding transcriptional regulation. By combining experimental approaches and computational methods, we suggest that the entropy-driven binding of CR3 to the MLL site could be due to the diverse orientations of CR3 (Fig. 4). The influence of water molecule release resulting from helical formation of the IDP or strong electrostatic interactions with the ligand at the MLL site also cannot be ruled out. Changes in protein conformational entropy can contribute significantly to

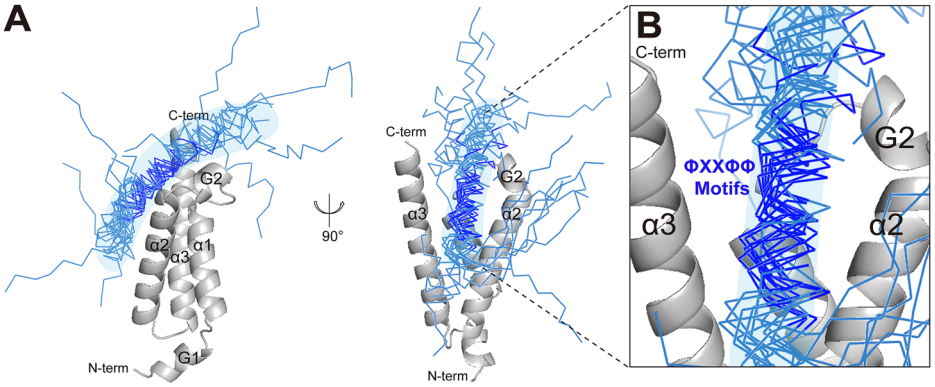

Fig. 8 | Predicted CBP-KIX and FOXO4-CR3 complex structures with AlphaFold3. A Complex model shows overlap of 13 predicted CR3s. **B** Enlarged view displays the ΦXXΦΦ motifs. KIX is colored in gray, CR3s are colored in light blue, and ΦXXΦΦ motifs are colored in blue. The structural models were visualized with PyMOL.

the overall free energy change of protein-ligand binding[32]. While 'selective promiscuity' typically refers to the permissive binding of unstructured regions, FOXO4-CR3 is distinct in that it retains promiscuous binding even though an induced-fit mechanism. Similar characteristics were also observed when FOXO3a-CR3 formed a secondary structure when bound to both CBP-KIX binding pockets[15]. Due to the heterogeneous nature of the complex, our CSP and PRE data may have limitations in defining more detailed structural features, and NOE and RDC measurements were technically challenging. Additional experimental data would help further clarify the structural features of the complex.

The K_d of FOXO3a-CR3 and CBP-KIX measured by ITC was 237 ± 40 μM, around 70-fold higher than that of FOXO4-CR3 and KIX[15]. The MLL site mutants also showed significantly higher K_d values in FOXO3a-CR3 than in FOXO4-CR3. Despite having similar sequences in the FOXO family, a significant difference in binding affinity is conferred from the CR3 sequences of FOXO3a and FOXO4. From a sequence point of view, only one ΦXXΦΦ motif ($FOXO3a_{624–628}$) exists in FOXO3a-CR3 ($FOXO3a_{610–644}$), and the sequence immediately following does not form an additional motif (Supplementary Fig. S13). As mentioned above, the KIX binding interface of FOXO3a-CR3 covers M624, S626, I627, and I628 in the ΦXXΦΦ motif, along with L632 and M633[15]. For FOXO4-CR3, we only observed a significant perturbation within the second ΦXXΦΦ motif. The relatively enhanced perturbations of the first motif were observed with $c\text{-}Myb_{mut}$, which mainly provides the MLL site for CR3 binding (Fig. 3). Comparing binding interfaces and affinities of FOXO4 and FOXO3a-CR3 to KIX, it seems that the subtle difference in the primary sequence significantly affects the binding properties.

The regulation of the interaction between FHD and CR3 in the presence or absence of the target DNA for FOXO4 activity has been previously studied[24]. FHD presents an overlapped binding surface to CR3 and DNA. FHD bound to target DNA can effectively release CR3 and form a transcription initiation complex containing coactivators such as CBP. Additionally, it is known that CR2 of FOXO3a also interacts with this transcriptional machinery[33], and the KIX binding affinity was synergistically enhanced in the presence of both CR2 and CR3[15]. Despite observing a much higher binding affinity of FOXO4-CR3 and KIX with a clear binding site preference in this study, we cannot rule out the possibility that CR2 also contributes to KIX binding with CR3. Further studies are needed to understand the mechanism of this interaction fully.

In summary, we thoroughly investigated FOXO4-CR3 binding to CBP-KIX. When interacting with the two hydrophobic pockets of KIX, the second ΦXXΦΦ motif present in FOXO4-CR3 is the predominant binding region with micromolar K_d. The helicity of FOXO4-CR3 is further enhanced when bound to the MLL site, suggesting MLL site preferential binding models. The dynamic nature of FOXO4-CR3 explains its promiscuity in binding to CBP-KIX. Our study provides detailed information about the unique binding properties of FOXO4-CR3 and CBP-KIX and expands the understanding of CBP recruitment via KIX-transactivation domain binding.

Methods

Sample preparation

The CBP-KIX (aa 586–672), KIX $c\text{-}Myb_{mut}$ (Y650A, A654Q, and Y658A), MLL_{mut} (I660A and L664A), C585 (KIX $c\text{-}Myb_{mut}$ C585), S670C (KIX $c\text{-}Myb_{mut}$ S670C), and 8aa (KIX $c\text{-}Myb_{mut}$-GGGSGGGS-CR3) genes were purchased from Integrated DNA Technologies (IDT), Inc. KIX and KIX MLL_{mut} were subcloned into the pET His6 TEV LIC cloning vector (2B-T) (a gift from Scott Gradia, Addgene plasmid #29666) and transformed into *E. coli* BL21 (DE3) cells. KIX $c\text{-}Myb_{mut}$, C585, S670C, and 8aa were subcloned into the pET His6 ProteinG TEV LIC cloning vector (1 P) (a gift from Scott Gradia, Addgene plasmid #29660) and transformed into *E. coli* BL21 (DE3) pLysS cells. Cells were grown in Luria-Bertani (LB) medium at 37 °C until an optical density of 0.8 at 600 nm was reached, and 1.0 mM of isopropyl-1-thio-b-D-galactopyrano side (IPTG) was added into the culture medium. For FOXO4-CR3 (aa 469–505) and M491A (FOXO4-CR3 M491A) expression, cells were cultured under identical conditions until the optical density reached 0.6 at 600 nm and induced with 0.5 mM IPTG[24].

After induction of the cells, KIX and KIX MLL_{mut} were incubated at 37 °C for 4 h, and KIX $c\text{-}Myb_{mut}$, C585, S670C, and 8aa were incubated at 18 °C for 20 h. Expressed proteins were purified using a Ni-NTA column (Cytiva) followed by gel filtration chromatography using a Hi-Load 16/600 Superdex 200 pg column (GE healthcare) on an AKTA pure system in a 20 mM MES, 100 mM NaCl buffer solution at pH 6.0. Glutathione-S-transferase (GST) and poly-histidine (His) tags were cleaved from protein samples by Tobacco Etch Virus (TEV) protease. ^{15}N-labeled and $^{13}C/^{15}N$-labeled samples were also expressed and purified with the same method using M9 media containing ^{13}C D-glucose and $^{15}NH_4Cl$. Protein expression and purification were the same as for the LB cultured protein.

Isothermal titration calorimetry analysis

ITC experiments were carried out in a 20 mM MES, 100 mM NaCl buffer solution at pH 6.0 using the Nano-ITC SV instrument (GIST, Gwangju). Titrations were performed by adding 10 μL of 400 μM KIX, KIX $c\text{-}Myb_{mut}$, and MLL_{mut} to 42 μM CR3 25 times at 25 °C; the first injection was not included in the final analysis. The interval between each injection was 300 s, and the stirring speed was 270 rpm. Experiments were repeated at least four times, and the error was derived from the results of each experiment. The dissociation constant (K_d) was obtained by fitting it to the 'Independent model' in the NanoAnalyze software (TA Instruments).

Nuclear magnetic resonance experiments

NMR experiments were performed using Bruker 900 MHz (KBSI, Ochang) and 600 MHz (GIST, Gwangju) NMR spectrometers equipped with cryogenic probes. NMR data were processed using Topspin software (Bruker) and analyzed with NMRFAM-Sparky software. The backbone assignment of KIX was obtained using $^1H–^{15}N$ HSQC, HNCO, HNCACO, HNCACB, and CBCACONH experiments[34]. The $^1H–^{15}N$ HSQC spectrum of CR3 was assigned using ^1H, ^{13}C, and ^{15}N chemical shift data from the Biological Magnetic Resonance Bank (BMRB code: 50259)[24]. The chemical shift index

data of 600 μM $^{13}C/^{15}N$-labeled FOXO4-CR3 in the presence of 300 μM KIX c-Myb_{mut} were obtained using a ^{13}C HNCA experiment. $\Delta\delta C_\alpha$ was calculated per residue by subtracting the free Cα chemical shift value reported in BMRB (BMRB code: 50259) from the Cα measured in the presence of KIX c-Myb_{mut}. For the $^{1}H–^{15}N$ HSQC titration experiments, unlabeled samples were added to ^{15}N-labeled samples (400 μM for KIX and KIX mutant, 600 μM for CR3 and M491A) at increasing concentrations at the indicated molar ratios. Average chemical shift change ($\Delta\delta_{avg}$) was calculated by the following equation:

$$\Delta\delta_{avg} = \sqrt{(\Delta\delta_H)^2 + \left(\frac{\Delta\delta_N}{5.88}\right)^2}$$

where $\Delta\delta_H$ and $\Delta\delta_N$ represent the chemical shift changes of the amide proton and nitrogen, respectively.

Paramagnetic relaxation enhancement (PRE) experiments were performed using paramagnetic probe, S-(1-oxyl-2,2,5,5-tetramethyl-2,5-dihydro-1H-pyrrol-3-yl)methyl methanesulfonothioate (MTSL), was used to label the cysteine residue KIX c-Myb_{mut} (C585 or S670C) or CR3 (C481), where 300 μM MTSL-labeled sample was added to 150 μM ^{15}N-labeled sample. The diamagnetic state was a solution containing 1.5 mM ascorbic acid, and the mixture was incubated at 25 °C for 3 h before performing NMR experiments. The peak intensities were measured and plotted as the ratio of the intensities in the oxidized state (I_{ox}, paramagnetic, without ascorbate) to those in the reduced state (I_{red}, diamagnetic, with ascorbate). Standard errors for the I_{ox}/I_{red} values were calculated by propagating the signal-to-noise ratio of the individual spectra using the equation below:

$$\frac{\delta I_{ox}/I_{red}}{I_{ox}/I_{red}} = \sqrt{\left(\frac{\delta I_{ox}}{I_{ox}}\right)^2 + \left(\frac{\delta I_{red}}{I_{red}}\right)^2}$$

where $\delta I_{ox}/I_{red}$ is the calculated error in the I_{ox}/I_{red} ratio, δI_{ox} is the noise level of the oxidized spectrum, and δI_{red} is the noise level of the reduced spectrum. All experiments were performed in a 20 mM MES, 100 mM NaCl buffer solution at pH 6.0 at 298 K.

CD spectroscopy

CD spectra were observed using a JASCO J-815 CD spectrometer (GIST, Gwangju) at 20 °C. KIX, KIX MLL_{mut}, KIX c-Myb_{mut}, and FOXO4-CR3 were dissolved in 20 mM MES, 100 mM NaCl buffer solution at pH 6.0 to a final concentration of 50 μM. All the spectra were collected from 200 nm to 250 nm at a scanning speed of 50 nm/min and with a spectral bandwidth of 1.0 nm for each sample. All the samples were incubated overnight at 4 °C. Secondary structure predictions were calculated by the BeStSel Web server[35].

Docking

We performed docking simulations of CBP-KIX and FOXO4-CR3 interactions with AlphaFold3, available at (https://alphafoldserver.com/)[36]. The complex structure was implemented by introducing the respective sequences of KIX and CR3. Simulations were conducted using random seeds. We also conducted docking simulations of CBP-KIX and FOXO4-CR3 interactions with AlphaFold2-multimer tool at ColabFold v1.5.2, available at (https://colab.research.google.com/github/sokrypton/ColabFold/blob/main/AlphaFold2.ipynb)[37,38]. Three recycles were performed without model relaxation. The images were taken at 300 dpi (by default). PyMOL was used for the visualization of docking models[39].

Reporting summary

Further information on research design is available in the Nature Portfolio Reporting Summary linked to this article.

Data availability

Representative complex model of KIX and CR3 (Fig. 8) generated using AlphaFold3 has been deposited in ModelArchive (https://doi.org/10.5452/ma-7trme). The source data behind the graphs can be found in Supplementary Data. All other data supporting the findings of this study are available from the corresponding author upon reasonable request.

Received: 7 March 2025; Accepted: 28 October 2025;
Published online: 11 December 2025

References

1. Chan, H. M. & La Thangue, N. B. p300/CBP proteins: HATs for transcriptional bridges and scaffolds. *J. Cell Sci.* **114**, 2363–2373 (2001).
2. Goodman, R. H. & Smolik, S. CBP/p300 in cell growth, transformation, and development. *Genes Dev.* **14**, 1553–1577 (2000).
3. Giordano, A. & Avantaggiati, M. L. p300 and CBP: Partners for life and death. *J. Cell. Physiol.* **181**, 218–230 (1999).
4. Chrivia, J. C. et al. Phosphorylated CREB binds specifically to the nuclear protein CBP. *Nature* **365**, 855–859 (1993).
5. Zor, T., De Guzman, R. N., Dyson, H. J. & Wright, P. E. Solution Structure of the KIX Domain of CBP Bound to the Transactivation Domain of c-Myb. *J. Mol. Biol.* **337**, 521–534 (2004).
6. Radhakrishnan, I. et al. Solution structure of the KIX domain of CBP bound to the transactivation domain of CREB: A model for activator:coactivator interactions. *Cell* **91**, 741–752 (1997).
7. De Guzman, R. N., Liu, H. Y., Martinez-Yamout, M., Dyson, H. J. & Wright, P. E. Solution structure of the TAZ2 (CH3) domain of the transcriptional adaptor protein CBP. *J. Mol. Biol.* **303**, 243–253 (2000).
8. Wang, F. et al. Synergistic Interplay between Promoter Recognition and CBP/p300 Coactivator Recruitment by FOXO3a. *ACS Chem. Biol.* **4**, 1017–1027 (2009).
9. Birkenkamp, K. U. & Coffer, P. J. Regulation of cell survival and proliferation by the FOXO (Forkhead box, class O) subfamily of Forkhead transcription factors. *Biochem. Soc. Trans.* **31**, 292–297 (2003).
10. Accili, D. & Arden, K. C. FoxOs at the Crossroads of Cellular Metabolism, Differentiation, and Transformation. *Cell* **117**, 421–426 (2004).
11. Essers, M. A. G. et al. FOXO transcription factor activation by oxidative stress mediated by the small GTPase Ral and JNK. *EMBO J.* **23**, 4802–4812 (2004).
12. Hornsveld, M., Dansen, T. B., Derksen, P. W. & Burgering, B. M. T. Re-evaluating the role of FOXOs in cancer. *Semin. Cancer Biol.* **50**, 90–100 (2018).
13. Ma, J., Matkar, S., He, X. & Hua, X. FOXO family in regulating cancer and metabolism. *Semin. Cancer Biol.* **50**, 32–41 (2018).
14. Greer, E. L. & Brunet, A. FOXO transcription factors at the interface between longevity and tumor suppression. *Oncogene* **24**, 7410–7425 (2005).
15. Wang, F. et al. Structures of KIX domain of CBP in complex with two FOXO3a transactivation domains reveal promiscuity and plasticity in coactivator recruitment. *Proc. Natl. Acad. Sci. USA* **109**, 6078–6083 (2012).
16. Kim, J., Dabin, A. + & Park, C.-J. Biophysical investigation of the dual binding surfaces of human transcription factors $FOXO_4$ and p53. *FEBS J.* **289**, 3163–3182 (2022).
17. Baar, M. P. et al. Targeted Apoptosis of Senescent Cells Restores Tissue Homeostasis in Response to Chemotoxicity and Aging. *Cell* **169**, 132–147.e16 (2017).
18. Spiegelman, B. M. & Heinrich, R. Biological control through regulated transcriptional coactivators. *Cell* **119**, 157–167 (2004).
19. Nasrin, N. et al. DAF-16 recruits the CREB-binding protein coactivator complex to the insulin-like growth factor binding protein 1 promoter in HepG2 cells. *Proc. Natl. Acad. Sci. USA* **97**, 10412–10417 (2000).

20. Senf, S. M., Sandesara, P. B., Reed, S. A. & Judge, A. R. P300 acetyltransferase activity differentially regulates the localization and activity of the FOXO homologues in skeletal muscle. *Am. J. Physiol. Cell Physiol.* **300**, 1490–1501 (2011).
21. van der Horst, A. et al. FOXO4 Is Acetylated upon Peroxide Stress and Deacetylated by the Longevity Protein hSir2SIRT1*. *J. Biol. Chem.* **279**, 28873–28879 (2004).
22. Dansen, T. B. et al. Redox-sensitive cysteines bridge p300/CBP-mediated acetylation and FoxO4 activity. *Nat. Chem. Biol.* **5**, 664–672 (2009).
23. Arai, M., Dyson, H. J. & Wright, P. E. Leu628 of the KIX Domain of CBP is a Key Residue for the Interaction with the MLL Transactivation Domain. *FEBS Lett.* **584**, 4500–4504 (2010).
24. Kim, J., Ahn, D. & Park, C. J. FOXO4 Transactivation Domain Interaction with Forkhead DNA Binding Domain and Effect on Selective DNA Recognition for Transcription Initiation. *J. Mol. Biol.* **433**, 166808 (2021).
25. Chu, W. T., Shammas, S. L. & Wang, J. Charge Interactions Modulate the Encounter Complex Ensemble of Two Differently Charged Disordered Protein Partners of KIX. *J. Chem. Theory Comput.* **16**, 3856–3868 (2020).
26. Hartlmüller, C., Spreitzer, E., Göbl, C., Falsone, F. & Madl, T. NMR characterization of solvent accessibility and transient structure in intrinsically disordered proteins. *J. Biomol. NMR* **73**, 305–317 (2019).
27. Brüschweiler, S., Konrat, R. & Tollinger, M. Allosteric communication in the KIX domain proceeds through dynamic repacking of the hydrophobic core. *ACS Chem. Biol.* **8**, 1600–1610 (2013).
28. Palazzesi, F., Barducci, A., Tollinger, M. & Parrinello, M. The allosteric communication pathways in KIX domain of CBP. *Proc. Natl. Acad. Sci. USA* **110**, 14237–14242 (2013).
29. Peiffer, A. L., Garlick, J. M., Joy, S. T., Mapp, A. K. & Brooks, C. L. Allostery in the dynamic coactivator domain KIX occurs through minor conformational micro-states. *PLoS Comput. Biol.* **18**, 1–19 (2022).
30. Huang, Y., Gao, M., Yang, F., Zhang, L. & Su, Z. Deciphering the promiscuous interactions between intrinsically disordered transactivation domains and the KIX domain. *Proteins Struct. Funct. Bioinforma.* **85**, 2088–2095 (2017).
31. Kim, J., Ahn, D. & Park, C. J. Biophysical investigation of the dual binding surfaces of human transcription factors FOXO4 and p53. *FEBS J.* **289**, 3163–3182 (2022).
32. Frederick, K. K., Marlow, M. S., Valentine, K. G. & Wand, A. J. Conformational entropy in molecular recognition by proteins. *Nature* **448**, 325–329 (2007).
33. So, C. W. & Cleary, M. L. MLL-AFX Requires the Transcriptional Effector Domains of AFX To Transform Myeloid Progenitors and Transdominantly Interfere with Forkhead Protein Function. *Mol. Cell. Biol.* **22**, 6542–6552 (2002).
34. Bax, A. & Grzesiek, S. Methodological advances in protein NMR. *NMR Proteins* 33–52, https://doi.org/10.1021/ar00028a001 (1993).
35. Micsonai, A. et al. BeStSel: A web server for accurate protein secondary structure prediction and fold recognition from the circular dichroism spectra. *Nucleic Acids Res.* **46**, W315–W322 (2018).
36. Abramson, J. et al. Accurate structure prediction of biomolecular interactions with AlphaFold 3. *Nature* **630**, 493–500 (2024).
37. Jumper, J. et al. Highly accurate protein structure prediction with AlphaFold. *Nature* **596**, 583–589 (2021).
38. Evans, R. et al. Protein complex prediction with AlphaFold-Multimer. *bioRxiv* https://doi.org/10.1101/2021.10.04.463034 (2022).
39. *The PyMOL Molecular Graphics System*. Version 1.8 Schrödinger LLC (2015).

Acknowledgements

We thank the high-field NMR facility at the Korea Basic Science Institute (KBSI, Ochang) and GIST Advanced Institute of Instrumental Analysis (GIST, Gwangju) for allowing us to use their NMR spectrometers. We appreciate Mr. Jiwoong Lee for helping with the ITC experiments. This work was supported by the National Research Foundation of Korea [grant 2021R1A2C100469, RS-2024-00411137, RS-2024-00440614, RS-2025-16068849], which is funded by the Korean government (MSIT).

Author contributions

J.H. data curation; formal analysis; investigation; visualization; writing-original draft; writing-review and editing. K.-S.R. formal analysis; investigation. C.-J.P. conceptualization; supervision; funding acquisition; project administration; writing-review and editing.

Competing interests

The authors declare no competing interests.

Additional information

Supplementary information The online version contains supplementary material available at https://doi.org/10.1038/s42003-025-09146-w.

Correspondence and requests for materials should be addressed to Chin-Ju Park.

Peer review information *Communications Biology* thanks Anastasia Zhuravleva and the other, anonymous, reviewer(s) for their contribution to the peer review of this work. Primary Handling Editors: Antonio Calabrese and Aylin Bircan. [A peer review file is available].